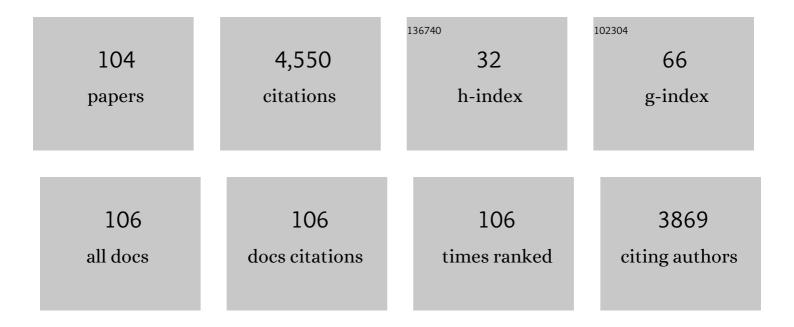
Gaspar Delso

List of Publications by Year in descending order

Source: https://exaly.com/author-pdf/7390716/publications.pdf Version: 2024-02-01



CASDAD DELSO

#	Article	IF	CITATIONS
1	Performance Measurements of the Siemens mMR Integrated Whole-Body PET/MR Scanner. Journal of Nuclear Medicine, 2011, 52, 1914-1922.	2.8	828
2	Tissue Classification as a Potential Approach for Attenuation Correction in Whole-Body PET/MRI: Evaluation with PET/CT Data. Journal of Nuclear Medicine, 2009, 50, 520-526.	2.8	663
3	NEMA NU 2-2012 performance studies for the SiPM-based ToF-PET component of the GE SIGNA PET/MR system. Medical Physics, 2016, 43, 2334-2343.	1.6	207
4	Zero <scp>TE</scp> <scp>MR</scp> bone imaging in the head. Magnetic Resonance in Medicine, 2016, 75, 107-114.	1.9	180
5	An overview of CEST MRI for non-MR physicists. EJNMMI Physics, 2016, 3, 19.	1.3	179
6	Design Features and Mutual Compatibility Studies of the Time-of-Flight PET Capable GE SIGNA PET/MR System. IEEE Transactions on Medical Imaging, 2016, 35, 1907-1914.	5.4	156
7	PET/MRI system design. European Journal of Nuclear Medicine and Molecular Imaging, 2009, 36, 86-92.	3.3	116
8	Evaluation of the attenuation properties of MR equipment for its use in a whole-body PET/MR scanner. Physics in Medicine and Biology, 2010, 55, 4361-4374.	1.6	112
9	Clinical Evaluation of Zero-Echo-Time MR Imaging for the Segmentation of the Skull. Journal of Nuclear Medicine, 2015, 56, 417-422.	2.8	111
10	PET–MR imaging using a tri-modality PET/CT–MR system with a dedicated shuttle in clinical routine. Magnetic Resonance Materials in Physics, Biology, and Medicine, 2013, 26, 25-35.	1.1	102
11	Clinical Evaluation of Zero-Echo-Time Attenuation Correction for Brain ¹⁸ F-FDG PET/MRI: Comparison with Atlas Attenuation Correction. Journal of Nuclear Medicine, 2016, 57, 1927-1932.	2.8	102
12	The effect of limited MR field of view in MR/PET attenuation correction. Medical Physics, 2010, 37, 2804-2812.	1.6	95
13	Evaluation of Atlas-Based Attenuation Correction for Integrated PET/MR in Human Brain: Application of a Head Atlas and Comparison to True CT-Based Attenuation Correction. Journal of Nuclear Medicine, 2016, 57, 215-220.	2.8	80
14	Evaluation of an Atlas-Based PET Head Attenuation Correction Using PET/CT & MR Patient Data. IEEE Transactions on Nuclear Science, 2013, 60, 3383-3390.	1.2	78
15	Whole-Body Nonenhanced PET/MR versus PET/CT in the Staging and Restaging of Cancers: Preliminary Observations. Radiology, 2014, 273, 859-869.	3.6	78
16	Comparison of 4-Class and Continuous Fat/Water Methods for Whole-Body, MR-Based PET Attenuation Correction. IEEE Transactions on Nuclear Science, 2013, 60, 3391-3398.	1.2	77
17	TNM Staging of Non–Small Cell Lung Cancer: Comparison of PET/MR and PET/CT. Journal of Nuclear Medicine, 2016, 57, 21-26.	2.8	65
18	Investigating the state-of-the-art in whole-body MR-based attenuation correction: an intra-individual, inter-system, inventory study on three clinical PET/MR systems. Magnetic Resonance Materials in Physics, Biology, and Medicine, 2016, 29, 75-87.	1.1	62

#	Article	IF	CITATIONS
19	Reduction of ¹⁸ F-FDG Dose in Clinical PET/MR Imaging by Using Silicon Photomultiplier Detectors. Radiology, 2018, 286, 249-259.	3.6	59
20	Anatomic Evaluation of 3-Dimensional Ultrashort-Echo-Time Bone Maps for PET/MR Attenuation Correction. Journal of Nuclear Medicine, 2014, 55, 780-785.	2.8	52
21	Quality control for quantitative multicenter wholeâ€body PET/MR studies: A NEMA image quality phantom study with three current PET/MR systems. Medical Physics, 2015, 42, 5961-5969.	1.6	51
22	Systematic Comparison of the Performance of Integrated Whole-Body PET/MR Imaging to Conventional PET/CT for ¹⁸ F-FDG Brain Imaging in Patients Examined for Suspected Dementia. Journal of Nuclear Medicine, 2014, 55, 923-931.	2.8	46
23	Intravoxel Incoherent Motion Protocol Evaluation and Data Quality in Normal and Malignant Liver Tissue and Comparison to the Literature. Investigative Radiology, 2016, 51, 90-99.	3.5	45
24	Clinical evaluation of a block sequential regularized expectation maximization reconstruction algorithm in 18F-FDG PET/CT studies. Nuclear Medicine Communications, 2017, 38, 57-66.	0.5	42
25	Black bone MRI with 3D reconstruction for the detection of skull fractures in children with suspected abusive head trauma. Neuroradiology, 2019, 61, 81-87.	1.1	40
26	Simulation Study of Tissue-Specific Positron Range Correction for the New Biograph mMR Whole-Body PET/MR System. IEEE Transactions on Nuclear Science, 2012, 59, 1900-1909.	1.2	38
27	Regional Accuracy of ZTE-Based Attenuation Correction in Static [18F]FDG and Dynamic [18F]PE2I Brain PET/MR. Frontiers in Physics, 2019, 7, .	1.0	38
28	PET/MR Outperforms PET/CT in Suspected Occult Tumors. Clinical Nuclear Medicine, 2017, 42, e88-e95.	0.7	37
29	Metal artifact reduction in patients with dental implants using multispectral three-dimensional data acquisition for hybrid PET/MRI. EJNMMI Physics, 2014, 1, 102.	1.3	36
30	Quantitative performance and optimal regularization parameter in block sequential regularized expectation maximization reconstructions in clinical 68Ga-PSMA PET/MR. EJNMMI Research, 2018, 8, 70.	1.1	36
31	Incorporation of Time-of-Flight Information Reduces Metal Artifacts in Simultaneous Positron Emission Tomography/Magnetic Resonance Imaging. Investigative Radiology, 2015, 50, 423-429.	3.5	35
32	Local resectability assessment of head and neck cancer: Positron emission tomography/MRI versus positron emission tomography/CT. Head and Neck, 2017, 39, 1550-1558.	0.9	35
33	Dose Optimization in TOF-PET/MR Compared to TOF-PET/CT. PLoS ONE, 2015, 10, e0128842.	1.1	30
34	Explicit Incorporation of Prior Anatomical Information Into a Nonrigid Registration of Thoracic and Abdominal CT and 18-FDG Whole-Body Emission PET Images. IEEE Transactions on Medical Imaging, 2007, 26, 164-178.	5.4	29
35	Multi-Atlas–Based Attenuation Correction for Brain 18F-FDG PET Imaging Using a Time-of-Flight PET/MR Scanner: Comparison with Clinical Single-Atlas– and CT-Based Attenuation Correction. Journal of Nuclear Medicine, 2016, 57, 1258-1264.	2.8	29
36	Improving PET/MR brain quantitation with template-enhanced ZTE. NeuroImage, 2018, 181, 403-413.	2.1	29

#	Article	IF	CITATIONS
37	Hybrid PET/MR Imaging: An Algorithm to Reduce Metal Artifacts from Dental Implants in Dixon-Based Attenuation Map Generation Using a Multiacquisition Variable-Resonance Image Combination Sequence. Journal of Nuclear Medicine, 2015, 56, 93-97.	2.8	28
38	Characterization of the impact to PET quantification and image quality of an anterior array surface coil for PET/MR imaging. Magnetic Resonance Materials in Physics, Biology, and Medicine, 2014, 27, 149-159.	1.1	26
39	Clinical Evaluation of PET Image Quality as a Function of Acquisition Time in a New TOF-PET/MRI Compared to TOF-PET/CT—Initial Results. Molecular Imaging and Biology, 2015, 17, 735-744.	1.3	26
40	A Quantitative Evaluation of Joint Activity and Attenuation Reconstruction in TOF PET/MR Brain Imaging. Journal of Nuclear Medicine, 2019, 60, 1649-1655.	2.8	26
41	Clinical evaluation of TOF versus non-TOF on PET artifacts in simultaneous PET/MR: a dual centre experience. European Journal of Nuclear Medicine and Molecular Imaging, 2017, 44, 1223-1233.	3.3	20
42	MR-driven metal artifact reduction in PET/CT. Physics in Medicine and Biology, 2013, 58, 2267-2280.	1.6	18
43	Cluster-based segmentation of dual-echo ultra-short echo time images for PET/MR bone localization. EJNMMI Physics, 2014, 1, 7.	1.3	18
44	ZTE MR-based attenuation correction in brain FDG-PET/MR: performance in patients with cognitive impairment. European Radiology, 2020, 30, 1770-1779.	2.3	18
45	Automated 3D MRI rendering of the craniofacial skeleton: using ZTE to drive the segmentation of black bone and FIESTA-C images. Neuroradiology, 2021, 63, 91-98.	1.1	18
46	How to Design Al-Driven Clinical Trials in Nuclear Medicine. Seminars in Nuclear Medicine, 2021, 51, 112-119.	2.5	17
47	Monte Carlo simulations of the count rate performance of a clinical wholeâ€body MR/PET scanner. Medical Physics, 2009, 36, 4126-4135.	1.6	16
48	Pitfalls and Limitations in Simultaneous PET/MRI. Seminars in Nuclear Medicine, 2015, 45, 552-559.	2.5	16
49	Multi-technique hybrid imaging in PET/CT and PET/MR: what does the future hold?. Clinical Radiology, 2016, 71, 660-672.	0.5	16
50	Effect of Time-of-Flight Information on PET/MR Reconstruction Artifacts: Comparison of Free-breathing versus Breath-hold MR-based Attenuation Correction. Radiology, 2017, 282, 229-235.	3.6	16
51	PET image reconstruction using physical and mathematical modelling for time of flight PET-MR scanners in the STIR library. Methods, 2021, 185, 110-119.	1.9	16
52	Preliminary study of the detectability of coronary plaque with PET. Physics in Medicine and Biology, 2011, 56, 2145-2160.	1.6	15
53	Clinical image quality perception and its relation to NECR measurements in PET. EJNMMI Physics, 2014, 1, 103.	1.3	15
54	Feasibility of ¹⁸ F-FDG Dose Reductions in Breast Cancer PET/MRI. Journal of Nuclear Medicine, 2018, 59, 1817-1822.	2.8	14

#	Article	IF	CITATIONS
55	Preliminary evaluation of image quality in a new clinical ToF-PET/MR scanner. EJNMMI Physics, 2014, 1, A41.	1.3	13
56	Pulmonary nodule detection in oncological patients – Value of respiratory-triggered, periodically rotated overlapping parallel T2-weighted imaging evaluated with PET/CT-MR. European Journal of Radiology, 2018, 98, 165-170.	1.2	13
57	Effect of Attenuation Correction on Regional Quantification Between PET/MR and PET/CT: A Multicenter Study Using a 3-Dimensional Brain Phantom. Journal of Nuclear Medicine, 2016, 57, 818-824.	2.8	11
58	Clinical Evaluation of ¹¹ C-Met-Avid Pituitary Lesions Using a ZTE-Based AC Method. IEEE Transactions on Radiation and Plasma Medical Sciences, 2019, 3, 504-508.	2.7	10
59	68Ga-PSMA-11 dose reduction for dedicated pelvic imaging with simultaneous PET/MR using TOF BSREM reconstructions. European Radiology, 2020, 30, 3188-3197.	2.3	10
60	Intra-individual comparison of PET/CT with different body weight-adapted FDG dosage regimens. Acta Radiologica Open, 2015, 4, 204798161456007.	0.3	9
61	How does PET/MR work? Basic physics for physicians. Abdominal Imaging, 2015, 40, 1352-1357.	2.0	9
62	Automated Segmentation of the Craniofacial Skeleton With "Black Bone―Magnetic Resonance Imaging. Journal of Craniofacial Surgery, 2020, 31, 1015-1017.	0.3	9
63	MR Image Based Approach for Metal Artifact Reduction in X-Ray CT. Scientific World Journal, The, 2013, 2013, 1-8.	0.8	8
64	The Effect of Susceptibility Artifacts Related to Metallic Implants on Adjacent-Lesion Assessment in Simultaneous TOF PET/MR. Journal of Nuclear Medicine, 2017, 58, 1167-1173.	2.8	8
65	Value of PET/MRI for assessing tumor resectability in NSCLC—intra-individual comparison with PET/CT. British Journal of Radiology, 2018, , 20180379.	1.0	8
66	Superresolution spatial compounding techniques with application to 3D breast ultrasound imaging. , 2006, , .		7
67	Comparison of 4-class and continuous fat/water methods for whole-body, MR-based PET attenuation correction. , 2012, , .		7
68	Repeatability of ZTE Bone Maps of the Head. IEEE Transactions on Radiation and Plasma Medical Sciences, 2018, 2, 244-249.	2.7	7
69	Three-dimensional magnetic resonance imaging ultrashort echo-time cones for assessing lung density in pediatric patients. Pediatric Radiology, 2021, 51, 57-65.	1.1	7
70	Free Form Deformations Guided by Gradient Vector Flow: A Surface Registration Method in Thoracic and Abdominal PET-CT Applications. Lecture Notes in Computer Science, 2003, , 224-233.	1.0	7
71	Technical and methodological aspects of PET/MR. Clinical and Translational Imaging, 2013, 1, 11-16.	1.1	6
72	MR Performance Comparison of a PET/MR System Before and After SiPM-Based Time-of-Flight PET Detector Insertion. IEEE Transactions on Nuclear Science, 2016, 63, 2419-2423.	1.2	6

#	Article	IF	CITATIONS
73	The impact of atlas-based MR attenuation correction on the diagnosis of FDG-PET/MR for Alzheimer's diseases— A simulation study combining multi-center data and ADNI-data. PLoS ONE, 2020, 15, e0233886.	1.1	6
74	Preliminary Evaluation of MR Image Quality in a New Clinical ToF-PET/MR System. IEEE Transactions on Nuclear Science, 2015, 62, 600-603.	1.2	5
75	The Effect of Defective PET Detectors in Clinical Simultaneous [18F]FDG Time-of-Flight PET/MR Imaging. Molecular Imaging and Biology, 2017, 19, 626-635.	1.3	5
76	Semiautomatic Algorithm for Lymph Node Analysis Corrected for Partial Volume Effects in Combined Positron Emission Tomography-Computed Tomography. Molecular Imaging, 2010, 9, 7290.2010.00019.	0.7	4
77	PET/MRI: Attenuation Correction. , 2018, , 53-75.		4
78	Clinical evaluation of PET image quality as a function of acquisition time in a new TOF-PET/MR compared to TOF-PET/CT - initial results. EJNMMI Physics, 2015, 2, A76.	1.3	3
79	4D Flow Magnetic Resonance Imaging for Left Atrial Haemodynamic Characterization and Model Calibration. Lecture Notes in Computer Science, 2021, , 156-165.	1.0	3
80	Improving the robustness of MOLLI T1 maps with a dedicated motion correction algorithm. Scientific Reports, 2021, 11, 18546.	1.6	3
81	Imaging of Bone in the Head and Neck Region, is There More Than CT?. Current Radiology Reports, 2022, 10, 69-82.	0.4	3
82	Curvilinear Component Analysis for high-dimensional data representation: II. Examples of additional mapping constraints in specific applications. Lecture Notes in Computer Science, 1999, , 635-644.	1.0	2
83	A Positron Emission Tomograph based on LSO-APD modules with a sampling ADC read-out system for a students' advanced laboratory course. Zeitschrift Fur Medizinische Physik, 2012, 22, 143-149.	0.6	2
84	Generation of pseudo-CT from a single MRI for PET/MR attenuation correction purposes. EJNMMI Physics, 2014, 1, A74.	1.3	2
85	Zero TEMR bone imaging in the head. Magnetic Resonance in Medicine, 2016, 75, spcone-spcone.	1.9	2
86	Implementation of Image Reconstruction for GE SIGNA PET/MR PET Data in the STIR Library. , 2018, , .		2
87	PET/MR System Design. , 2014, , 1-19.		2
88	Evaluation and clinical quantification of neoplastic lesions and physiological structures in TOF- versus non-TOF-PET/MRI: a pilot study. Quarterly Journal of Nuclear Medicine and Molecular Imaging, 2022, 65, .	0.4	2
89	PET/CT image denoising and segmentation based on a multi observation and a multi scale Markov tree model. , 2013, , .		1

90 Metal artifact reduction from CT images using complementary MR images. , 2013, , .

1

#	Article	IF	CITATIONS
91	Dynamic comparison of PET imaging performance between state-of-the-art ToF-PET/CT and ToF-PET/MR scanners. EJNMMI Physics, 2014, 1, A75.	1.3	1
92	Suppression of Metal Artefacts in CT Using Virtual Singorams and Corresponding MR Images. Current Science, 2017, 112, 1505.	0.4	1
93	Enhancing Distraction Osteogenesis With Carbon Fiber Reinforced Polyether Ether Ketone Bone Pins and a Three-Dimensional Printed Transfer Device to Permit Artifact-Free Three-Dimensional Magnetic Resonance Imaging. Journal of Craniofacial Surgery, 2021, 32, 360-364.	0.3	1
94	Evaluation of multifunctional imaging parameters in gastro-oesophageal cancer using F-18-FDG-PET/CT with integrated perfusion CT. Quarterly Journal of Nuclear Medicine and Molecular Imaging, 2018, , .	0.4	1
95	Reproducibility of Standardized Uptake Values Including Volume Metrics Between TOF-PET-MR and TOF-PET-CT. Frontiers in Medicine, 2022, 9, 796085.	1.2	1
96	COMPUTER-ASSISTED ECHOCARDIOGRAPHIC DIAGNOSIS. IFAC Postprint Volumes IPPV / International Federation of Automatic Control, 2002, 35, 241-245.	0.4	0
97	Evaluation of MR acquisition strategies for MR based attenuation correction. , 2013, , .		0
98	Image processing methods for PET/MR multi-modality imaging: Initial study regarding binding of MR images. , 2013, , .		0
99	Study of the correlation of IVIM parameter maps with FDG PET. Nuclear Instruments and Methods in Physics Research, Section A: Accelerators, Spectrometers, Detectors and Associated Equipment, 2014, 734, 201-205.	0.7	0
100	Dynamic brain PET/MR using TOF reconstruction. EJNMMI Physics, 2015, 2, A60.	1.3	0
101	Zero Echo Time MRAC on FDG-PET/MR Maintains Diagnostic Accuracy for Alzheimer's Disease; A Simulation Study Combining ADNI-Data. Frontiers in Neuroscience, 2020, 14, 569706.	1.4	0
102	Spatially Constrained Deep Learning Approach for Myocardial T1 Mapping. Lecture Notes in Computer Science, 2021, , 148-158.	1.0	0
103	Role of intravoxel incoherent motion parameters in gastroesophageal cancer: relationship with 18F-FDG-positron emission tomography, computed tomography perfusion and magnetic resonance perfusion imaging parameters. Quarterly Journal of Nuclear Medicine and Molecular Imaging, 2021, 65, 178-186.	0.4	0
104	CT and PET Registration Using Deformations Incorporating Tumor-Based Constraints. Lecture Notes in Computer Science, 2005, , 1-12.	1.0	0